Optical Absorptions and Raman Scattering of Metalloporphycenes Reveal Electronic and Vibronic Properties Distinct from Those of Metalloporphyrins

W. Anthony Oertling,*,† Weishih Wu, Juan J. Lôpez-Garriga,‡ Younkyoo Kim, and Chi K. Chang*

Contribution from the Department of Chemistry and the LASER Laboratory, Michigan State University, East Lansing, Michigan 48824. *Received March 19, 1990*

Abstract: The newly synthesized metalloporphycenes represent a class of molecules that are structural isomers of metalloporphyrins. In particular, the Ni^{II} and Cu^{II} complexes of 2,7,12,17-tetrapropylporphycene (NiPPC and CuPPC) display UV–visible absorption and resonance Raman (RR) spectra superficially like those of analogous complexes of octaethylporphyrin (OEP). However, close examination of absorption band positions and spectral shifts caused by metal substitution and ring bromination, as well as relative oscillator strengths, suggest that, unlike those of metalloporphyrins, the $\pi \rightarrow \pi^*$ states of NiPPC and CuPPC are adequately defined by one-electron wave functions. Thus, the π-electron configuration interaction that gives rise to Gouterman's Q and B metalloporphyrin excited states is weak in metalloporphycenes. Rather, these novel complexes appear to be a near-perfect example of Platt's "long-field" molecules (Platt, J. R. *J. Chem. Phys.* **1950**, *18*, 1168–1173). Raman spectra in resonance with the major absorptions of CuPPC show little evidence of Jahn–Teller or Herzberg–Teller coupling. Thus, the rich vibronic coupling present in metalloporphyrins giving rise to the celebrated anomalously polarized scattering (Spiro, T. G; Strekas, T. C. *Proc. Natl. Acad. Sci. U.S.A.* **1972**, *69*, 2622–2626) most likely does not complicate the spectra of metalloporphycenes. Vibrational analyses of RR spectra of specifically deuterated derivatives of NiPPC give some insight into the normal mode compositions. Metal substitution reveals structure-sensitive vibrations and suggests that frequency–structure correlations will be possible when more X-ray crystal data are available. Similarly to hemes, both UV–visible and RR spectra of FePPC derivatives demonstrate sensitivity to iron spin and oxidation state that suggests overlap of the iron d_{xz} and d_{yz} and the porphycene π orbitals. Once properly calibrated by comparison to results from magnetic-based techniques, the RR frequencies of the macrocycle will be a reliable probe of the metal electronic state in iron porphycenes.

Introduction

Porphycene, a tetrapyrrole macrocycle recently synthesized by Vogel et al.,[1] is a structural isomer of porphine, the parent compound of porphyrins. The limited solubility of porphycene and metalloporphycene led Vogel and co-workers[2] to develop the synthesis of 2,7,12,17-tetrapropylporphycene (PPC). This compound is expected to assume in porphycene investigations a role similar to that of octaethylporphyrin (OEP) in studies of model porphyrin complexes. Porphycenes are likely agents for photodynamic therapy owing to their absorption of wavelengths above 620 nm and other photophysical properties.[3] For this reason the electronic properties of these novel macrocycles are of interest. Figure 1 compares the structures of CuPPC and CuOEP.

In order to interpret vibrational spectra of naturally occurring pigments (e.g. chlorophyll) possessing tetrapyrrole-derived structures of symmetry lower than that of metallooctaethylporphyrin (MOEP), several groups have carried out systematic studies of the effects of symmetry lowering on the macrocyclic vibrational properties of metallooctaethylchlorins (MOEC)[4a-d] and metallopheophorbides.[4e] Similarly the spectroscopic properties of metal complexes of bacteriochlorins and bacteriopheophorbides[5] should progressively approach those of bacteriochlorophyll. In this spirit, metalloporphycene represents an example of a macrocycle of true D_{2h} symmetry which is approximated by metallobacteriochlorins[5b] and heme *a*.[6] Furthermore, the bipyrrole $C_{a'}C_{a'}$ bond is a structural feature of the corrin macrocycle; thus, cobalt complexes of porphycene derivative may model some aspects of vitamin B_{12}. Recently, Renner et al.[7] have characterized the NiPPC anion radical and compared the redox properties of this compound to other nickel porphinoid models of coenzyme F_{430} from methanogenic bacteria.

Resonance Raman spectroscopy (RR) has been applied extensively to synthetic MOEP,[8] MOEC,[4] metallobacteriochlorins,[5] and metallocorphinoids.[9] It has been used to study redox-altered states of MOEP and MOEC including π cation[10] and anion[11]

† Present address: Inorganic and Structural Chemistry Group, INC-4, Mail Stop C-345, Los Alamos National Laboratory, Los Alamos, New Mexico 87545.

‡ Present address: Department of Chemistry University of Puerto Rico, Mayagüez, Mayagüez, Puerto Rico 00708.

(1) Vogel, E.; Köcher, M.; Schmickler, H.; Lex, J. *Angew. Chem., Int. Ed. Engl.* **1986**, *25*, 257–259.

(2) (a) Vogel, E.; Balci, M.; Pramod, K.; Koch, P.; Lex, J.; Ermer, O. *Angew. Chem., Int. Ed. Engl.* **1987**, *26*, 928–931. (b) Vogel, E.; Köcher, M.; Balci, M.; Teichler, I.; Lex, J.; Schmickler, H.; Ermer, O. *Angew. Chem., Int. Ed. Engl.* **1987**, *26*, 931–934. (c) Wehrle, B.; Limbach, H.-H.; Köcher, M.; Ermer, O.; Vogel, E. *Angew. Chem., Int. Ed. Engl.* **1987**, *26*, 934–936. (d) Schülpmann, J.; Huber, M.; Toporowicz, M.; Köcher, M.; Vogel, E.; Levanon, H.; Möbius, K. *J. Am. Chem. Soc.* **1988**, *110*, 8566–8567. (e) Vogel, E.; Köcher, M.; Lex, J.; Ermer, O. *Isr. J. Chem.* **1989**, *29*, 257–266.

(3) (a) Aramendia, P. F.; Redmond, R. W.; Novell, S.; Schuster, W.; Braslavsky, S. E.; Schaffner, K.; Vogel, E. *Photochem. Photobiol.* **1986**, *44*, 555–559. (b) Ofir, H.; Regev, A.; Levanon, H.; Vogel, E.; Köcher, M.; Balci, M. *J. Phys. Chem.* **1987**, *91*, 2686–2688. (c) Levanon, H.; Toporowicz, M.; Ofir, H.; Fessenden, R. W.; Paritosh, K. D.; Vogel, E.; Köcher, M.; Pramod, K. *J. Phys. Chem.* **1988**, *92*, 2429–2433. (d) Redmond, R. W.; Valduga, G.; Novell, S.; Braslavsky, S. E.; Schaffner, K.; Vogel, E.; Pramod, K.; Köcher, M. *J. Photochem. Photobiol. B* **1989**, *3*, 193–207.

(4) (a) Ozaki, Y.; Iriyama, K.; Ogoshi, H.; Ochiai, T.; Kitagawa, T. *J. Phys. Chem.* **1986**, *90*, 6105–6112. (b) Boldt, N. J.; Donohoe, R. J.; Birge, R. R.; Bocian, D. F. *J. Am. Chem. Soc.* **1987**, *109*, 2284–2298. (c) Andersson, L. A.; Loehr, T. N.; Stershic, M. T.; Stolzenberg, A. M. *Inorg. Chem.* **1990**, *29*, 2278–2285. (d) Fonda, H. N.; Oertling, W. A.; Salehi, A.; Chang, C. K.; Babcock, G. T. *J. Am. Chem. Soc.* **1990**, *112*, 9497–9507. (e) Anderson, L. A.; Loehr, T. M.; Cotton, T. M.; Simpson, D. J.; Smith, K. M. *Biochim. Biophys. Acta* **1989**, *974*, 163–179.

(5) (a) Donohoe, R. J.; Frank, H. A.; Bocian, D. F. *Photochem. Photobiol.* **1988**, *48*, 531–537. For a recent review, see: (b) Schick, A. G.; Bocian, D. F. *Biophys. Biochim. Acta.* **1987**, *895*, 127–154.

(6) Woodruff, W. H.; Kessler, R. J.; Ferris, N. S.; Dallinger, R. F. *Adv. Chem. Ser.* **1982**, *201*, 625–659.

(7) Renner, M. W.; Forman, A.; Wu, W.; Chang, C. K.; Fajer, J. *J. Am. Chem. Soc.* **1989**, *111*, 8618–8621.

(8) For a recent review, see: Kitagawa, T.; Ozaki, Y. *Struct. Bonding* **1987**, *64*, 71–114.

(9) Shelnutt, J. A. *J. Am. Chem. Soc.* **1987**, *109*, 4169–4173.

(10) (a) Oertling, W. A.; Salehi, A.; Chung, Y. C.; Leroi, G. E.; Chang, C. K.; Babcock, G. T. *J. Phys. Chem.* **1987**, *91*, 5887–5898. (b) Salehi, A.; Oertling, W. A.; Fonda, H. N.; Chang, C. K.; Babcock, G. T. *Photochem. Photobiol.* **1988**, *48*, 525–530. (c) Donohoe, R. J.; Duchowski, J. K.; Bocian, D. F. *J. Am. Chem. Soc.* **1988**, *110*, 6119–6124. (d) Oertling, W. A.; Salehi, A.; Chang, C. K.; Babcock, G. T. *J. Phys. Chem.* **1989**, *93*, 1311–1319. (e) Czernuszewicz, R. S.; Macor, K. A.; Li, X.-Y.; Kincaid, J. R.; Spiro, T.-G. *J. Am. Chem. Soc.* **1989**, *111*, 3860–3969.

0002-7863/91/1513-127$02.50/0

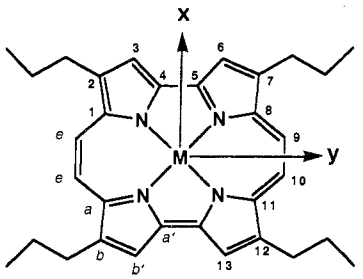

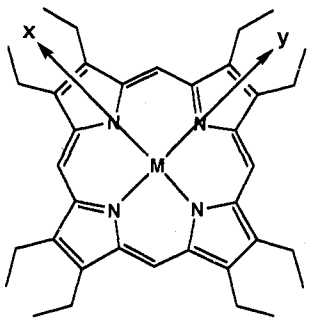

Figure 1. Structures of copper 2,7,12,17-tetrapropylporphycene (CuPPC) and copper 1,2,6,7,11,12,16,17-octaethyporphyrin (CuOEP). Symmetry axes and the carbon labeling scheme are also shown.

radicals. These model compound studies have helped interpret RR results from a number of important natural systems including heme proteins,[12] reaction center chlorophyll and bacteriochlorphyll,[13] coenzyme F_{430},[14] and vitamin B_{12}.[15] One of the virtues of the RR technique lies in its applicability to all of these systems. The technique offers a range of information regarding structure and electronic properties and is amenable to the study of dynamic processes via time-resolved applications. Interpretation of results from complex biological systems and from sophisticated techniques requires thorough grounding in basic spectroscopic study. For these reasons, we describe here the UV–visible and resonance Raman (RR) spectra of metal-substituted and selectively deuterated PPC compounds and compare them to the well-known spectra of analogous OEP species.

Materials and Methods

CuPPC and NiPPC Compounds. The free base 2,7,12,17-tetrapropylporphycene (H_2PPC) was synthesized according to Vogel et al.[2a] The metal complexation procedures for Ni^{II} and Cu^{II} were described earlier.[7] Selective deuteration at the C_e positions, NiPPC-*9,10,19,20*-d_4 (abbreviated NiPPC-d_4(et)), was achieved by synthesis as described earlier.[7,16] Deuteration at the C_b, positions, NiPPC-*3,6,13,16*-d_4 (NiPPC-d_4(py)), was prepared by refluxing H_2PPC in deuterated acetic acid (d_1, 99.9%) in the presence of nickel acetate and sodium acetate under nitrogen for 8 h. The ^{1}H NMR indicated that the protons on pyrrole rings were replaced by deuteriums almost quantitatively while only 17% replacement occurred at ethylene bridge positions.

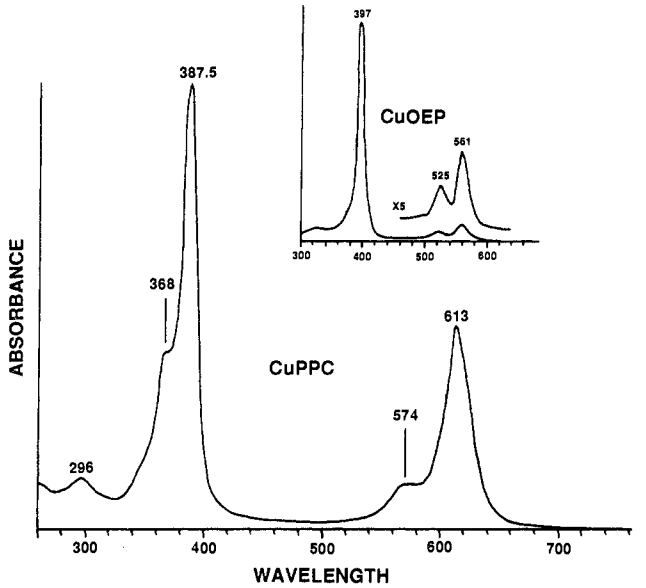

Figure 2. UV–visible absorption spectra of CuPPC and CuOEP (inset) in CH_2Cl_2. Concentrations are approximately 75 μM, the cell path is 2.0 mm, and the wavelength is measured in nm.

3,6,13,16-Tetrabromo-2,7,12,17-tetrapropylporphycene. Bromination at the $C_{b'}$ positions (see Figure 1) was accomplished by the following procedures. To a magnetically stirred solution of the free base porphycene in chloroform was added drop-by-drop a solution of bromine in chloroform. The yield of mono-, di-, tri-, and tetrabromoporphycene was dependent on the amount of bromine added. The reaction was easily monitored by TLC developed with hexane/CH_2Cl_2 (1:1). At the end of reaction the solvent was evaporated and the residue was chromatographed on preparative TLC plates (hexane/CH_2Cl_2). ^{1}H NMR (d_6-acetone) δ 9.80 (4 H), 3.90 (8 H, t, $CH_2CH_2CH_3$), 2.20 (8 H, m, $CH_2CH_2CH_3$), 1.78 (12 H, t, $CH_2CH_2CH_3$). UV–vis (CH_2Cl_2) λ_{max} (rel intensity) 381 (1.00), 389 (sh, 0.98), 592 (0.32), 638 (0.19), 683 nm (0.27). Anal. ($C_{32}H_{32}Br_4N_4$) C, H, N. The Ni(II) and Cu(II) complexes were prepared in the same manner as described above.

Iron(III) Tetrapropylporphycene Chloride (ClFe^{III}PPC). To a solution of the free base porphycene (30 mg) in acetic acid (20 mL) was added ferric chloride (30 mg) and sodium acetate (5 mg). After refluxing for 10 h the solution was cooled and partitioned in methylene chloride (100 mL) and water (60 mL). The organic layer was separated, washed three times with water, and evaporated. The residue was chromatographed on a silica gel column and eluted with methylene chloride first to remove the unreacted porphycene (13 mg, 44%) and then with MeOH (2%)/CH_2Cl_2 to collect the dark-green iron(III) complex. The fraction containing iron(III) porphycene was washed with hydrochloric acid (2 N), brought to dryness, and crystallized from CH_2Cl_2 and hexane. Yield 18 mg (54%); UV–vis, λ_{max} (rel intensity), 364 (1.00), 617 nm (0.52); MS, m/z 531 (M^+); mp >300 °C. Titration of the ferric chloride complex with *N*-methylimidazole (Im) resulted in (Im)$_2$Fe^{III}PPCCl. Reduction of (Im)$_2$Fe^{III}PPCCl was accomplished chemically by two methods. First, a CH_2Cl_2 solution of (Im)$_2$Fe^{III}PPCCl was made anaerobic by several freeze–pump–thaw cycles and titrated with hydrazine hydrate. Second, an anaerobic CH_2Cl_2 solution of (Im)$_2$Fe^{III}PPCCl was reduced by shaking with aqueous sodium dithionite. Both preparations resulted in ferrous adducts with similar UV–visible spectra. The first preparation was used for the RR measurement and the absorption spectrum is inset in Figure 8.

UV–visible absorbance measurements were recorded on a Perkin-Elmer λ-5 spectrophotometer. Resonance Raman spectra were obtained from 0.1–0.5 mM samples in CH_2Cl_2 solution in cylindrical quartz spinning cells. The Raman equipment included a Spex 1401 Ramalog with PMT detection, a Spex 1877 Triplemate with EG&G Model 1420 detector and OMA II electronics, and a Spex 1877 B outfitted with a EG&G Model 1421 detector and OMA III computer. The laser systems included a Spectra Physics Model 164 argon ion and model 375 dye laser (to provide wavelengths of 630.0 and 613.0 nm), a Coherent Innova 100 argon (363.8 nm) and Innova 90 krypton (568.2 and 406.7 nm) ion lasers, and a Quanta Ray DCR-2A Nd:YAG and PDL-2 dye laser (390 and 355 nm). In all cases, the stability of each particular complex to the laser irradiation employed was confirmed by identical UV–visible ab-

(11) (a) Ksenofontova, N. M.; Maslov, V. G.; Sidorov, A. N.; Bobovich, Y. S. *Opt. Spectrosc.* **1976**, *40*, 462–465. (b) Teraoka, J.; Hashimoto, S.; Sugimoto, H.; Kitagawa, T. *J. Am. Chem. Soc.* **1987**, *109*, 180–184. (c) Donohoe, R. J.; Atamian, M.; Bocian, D. F. *J. Am. Chem. Soc.* **1987**, *109*, 5593–5599.

(12) Spiro, T. G. In *Iron Porphyrins*; Lever, A. B. P., Gray, H. B., Eds.; Addison-Wesley: Reading, MA, 1983; Part 2, pp 89–159.

(13) (a) Lutz, M.; Robert, B. In *Biological Applications of Raman Spectroscopy*; Spiro, T. G., Ed.; John Wiley & Sons: New York, 1988; pp 347–411. (b) Callahan, P. M.; Cotton, T. M. *J. Am. Chem. Soc.* **1987**, *109*, 7001–7007.

(14) (a) Schiemke, A. K.; Eirich, L. D.; Loehr, T. M. *Biochim. Biophys. Acta* **1983**, *748*, 143–150. (b) Schiemke, A. K.; Scott, R. A.; Shelnutt, J. A. *J. Am. Chem. Soc.* **1988**, *110*, 1645–1646.

(15) (a) Mayer, E.; Gardiner, D. J.; Hester, R. E. *Mol. Phys.* **1973**, *26*, 783–787. (b) Salama, S.; Spiro, T. G. *J. Raman Spectrosc.* **1977**, *6*, 57–60.

(16) Insertion of Ni^{II} to the deuterated macrocycle in HOAc resulted in a 10% loss of the deuterium for hydrogen.

Table I. UV-Visible Absorptions (nm) of Metalloporphycenes and Metalloporphyrins and Assignment of Electronic Transitions of MPPC

NiPPC[a]	CuPPC	Cu-Br_4PPC	one-electron ψ	symmetry
601.5	613	631	$b_{1u}b_{2g}$	$B_{3u}(x)$
563 (sh)	574	586	$b_{1u}b_{3g}$	$B_{2u}(y)$
388	387.5	388	a_ub_{2g}	$B_{2u}(y)$
369 (sh)	368 (sh)	369 (sh)	a_ub_{3g}	$B_{3u}(x)$

NiOEP[b]	CuOEP	NiDPDME[c]	Ni-2,4-Br_2DPDME
551	561	549.5	553
516	525	514	518
391	397	390.5	395

[a] Band positions of CH_2Cl_2 solutions were determined by inspection of expanded spectra, as well as first- and second-derivative spectra. [b] Band positions of CH_2Cl_2 solutions were determined from multiple runs of each absorption spectrum. [c] Band positions of $CHCl_3$ solutions as reported in ref 23.

sorption spectra before and after the Raman measurements.

Results and Discussion

In order to understand the electronic and vibrational aspects of the porphycene macrocycle and to compare them to the porphyrins, we first focus on the UV-visible absorptions of four-coordinate divalent transition-metal complexes that exist in a single spin state and do not exhibit metal-macrocycle π bonding. In this way we establish the nature of the $\pi \rightarrow \pi^*$ electronic states of the ring. Next, resonance Raman results are used to evaluate the vibrational and vibronic properties of this new class of complexes, and comparison of the vibrational frequencies to the known structural properties is used to identify interpretable trends. Finally, this combined analysis is applied to a more difficult case, namely iron complexes in various ligation, valence, and spin states.

UV-Visible Absorption Spectra. Figure 2 shows the UV-visible absorption spectrum of CuPPC and, for comparison, the spectrum of the analogous porphyrin compound, CuOEP (inset). The spectrum of the porphycene compound is superficially like that of the porphyrin species, but the oscillator strengths of the near-UV and visible bands are more nearly equal in the PPC complex. Also, the near-UV band of CuPPC is noticeably split into two components, and compared to that of CuOEP, this band is blue-shifted and the visible band is red-shifted in the CuPPC spectrum.

The UV-visible absorptions of the metalloporphyrins have been the subject of extensive study for many years. They arise for the most part from in-plane $\pi \rightarrow \pi^*$ transitions of the macrocycle which are described by the four-orbital model of Gouterman.[17] Shelnutt has more recently quantified certain aspects of the model.[18] Foundation for this work came from earlier attempts to explain the π-electron spectra of large conjugated ring molecules.[19-21] The model adequately explains the effects of variation of the central metal and peripheral substituents on the electronic structure of the macrocyclic complexes. Comparisons of these effects in metalloporphyrin spectra to those we observe in metalloporphycene spectra reveal fundamental differences.

Figure 3, parts A and B, shows absorption spectra of NiPPC and CuPPC. In order to resolve the key spectral features the first derivative of each spectrum is superimposed. Table I collects the band positions determined by inspection of expanded spectra, as well as first and second derivative spectra of NiPPC and CuPPC. Also included are band positions for the Cu^{II} complex of 3,6,13,16-Br_4PPC (i.e. Br is substituted for H at the $C_{b'}$ positions, Figure 1). These are compared to absorption maxima for the porphyrin complexes NiOEP, CuOEP, NiDPDME, and Ni-2,4-Br_4DPDME (DPDME = deuteroporphyrin IX dimethyl ester). The table illustrates that a change in the central metal or bromination at the ring periphery significantly shifts both the near-UV (Soret) and visible bands of the porphyrin complexes; however, these substitutions in the porphycene complexes shift only the

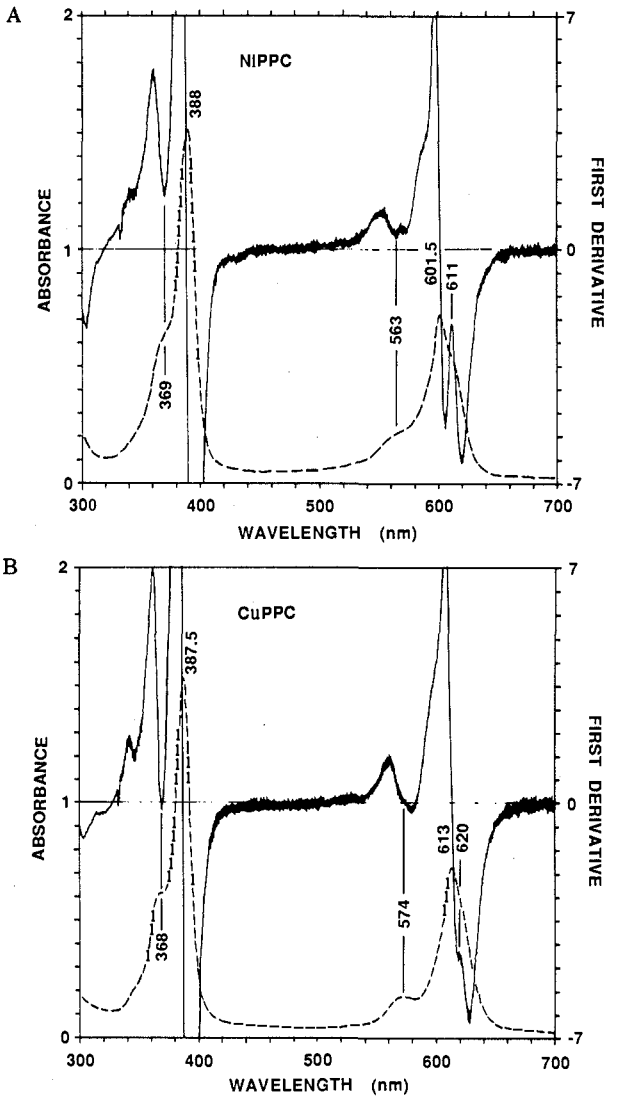

Figure 3. UV-visible absorption and first derivative absorption spectra of CuPPC and NiPPC in CH_2Cl_2. Spectra with the wavelength scale expanded ×2 as well as first and second derivative spectra similarly expanded were used to determine the wavelength of features labeled in the figure.

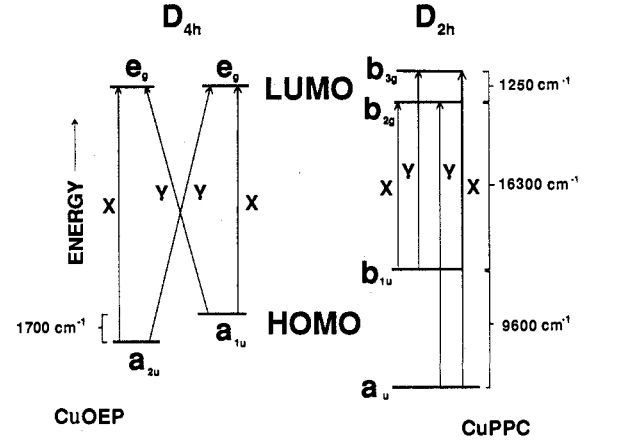

Figure 4. Schematic orbital energy level diagrams for CuOEP (D_{4h}) and CuPPC (D_{2h}).

(17) (a) Gouterman, M. *J. Chem. Phys.* **1959**, *30*, 1139-1161. (b) Gouterman, M. *J. Mol. Spectrosc.* **1961**, *6*, 138-163.
(18) (a) Shelnutt, J. A. *J. Phys. Chem.* **1984**, *88*, 4988-4992. (b) Shelnutt, J. A.; Ortiz, V. *J. Phys. Chem.* **1985**, *89*, 4733-4739.
(19) Simpson, W. T. *J. Chem. Phys.* **1949**, *17*, 1218-1221.
(20) (a) Platt, J. R. *J. Chem. Phys.* **1950**, *18*, 1168-1173. (b) Longuet-Higgins, H. C.; Rector, C. W.; Platt, J. R. *J. Chem. Phys.* **1950**, *18*, 1174-1181.
(21) (a) Pariser, R.; Parr, R. G. *J. Chem. Phys.* **1953**, *21*, 767-776. (b) Moffitt, W. *J. Chem. Phys.* **1954**, *22*, 1820-1829.

visible bands and leave the near-UV band positions virtually unchanged. This illustrates a basic difference in the electronic properties of metalloporphycenes and metalloporphyrins and is discussed below.

Electronic Properties. The differences in the electronic properties of metalloporphycene from those of metalloporphyrin are the consequence of the difference in point group symmetry. Figure 4 depicts an orbital energy level diagram for both metalloporphyrin (D_{4h}) and metalloporphycene (D_{2h}). For metalloporphyrin four essentially degenerate one-electron excited-state wave functions are heavily mixed by configuration interaction (CI) resulting in linear combinations usually referred to as the Q (visible) and B (Soret) states.[17] These are of $E_u(x,y)$ symmetry. The Q state transition is formally forbidden but gains intensity through vibronic coupling to the B state, which represents an allowed transition. In D_{4h} metalloporphyrins the x and y components of the Q and B states are degenerate, and each total wave function involves all four one-electron wave functions. The configuration interaction comes about primarily because the HOMO energy splitting is small compared to the electron interaction energy. The latter can be estimated by the observed energy difference between the B and Q transition energies and, by the data in Table I, is 7300 cm^{-1} for CuOEP. Shelnutt[18] estimates the energy difference between the a_{1u} and a_{2u} orbitals of CuOEP to be 1700 cm^{-1}. As a consequence of the electronic configuration, the spectral effects of substitution at the metal center or at the pyrrole ring periphery change *both* the Q and B transition energies. On going from NiOEP to CuOEP there is an expansion of the porphyrin core that results in an increase in the energy of the a_{2u} orbital relative to the a_{1u} and LUMO orbitals.[18] Thus, a red-shift occurs.

For metalloporphycene, on the other hand, the degeneracy of the LUMOs and the near degeneracy of the HOMOs are lifted. For CuPPC we estimate a 1250-cm^{-1} gap between the b_{2g} and b_{3g} orbitals and a 9600-cm^{-1} splitting between the a_u and b_{1u} orbitals. This results in four allowed transitions, each essentially one-electron exited-state wave functions. Table I assigns these transitions to the NiPPC, CuPPC, and Cu-Br_4PPC absorption spectra. According to this model, the effects of substitution are easily understood. Incorporation of Ni^{II} rather than Cu^{II} lowers the relative energy of the b_{1u} orbital by 300 cm^{-1} and causes a blue-shift of both the $B_{3u}(x)$ and $B_{2u}(y)$ transitions to the respective $b_{1u}b_{2g}$ and $b_{1u}b_{3g}$ excited states. On the other hand, tetrabromination at the $C_{b'}$ positions raises the b_{1u} energy by 400 cm^{-1} relative to that of the a_{1u} and the LUMOs, accounting for the observed red-shifts. Thus, the relative energy level of the b_{1u} orbital (which corresponds to the a_{2u} orbital in D_{4h} symmetry)[22a] increases in the series NiPPC, CuPPC, and Cu-Br_4PPC. This trend is most likely owing to expansion of the macrocycle. While increased core size on going from NiPPC to CuPPC is analogous to the OEP complexes, tetrabromination further increases the macrocycle core size because the bulky $C_{b'}$ substituents interact sterically.[2e] Although metal substitution and bromination of the ring may well change the absolute energies of all orbitals, neither substitution affects the *relative* energies of the a_u or the LUMOs, thus the near-UV transition energies do not change.[22b] Accordingly, in the absence of strong configuration interaction, the MO energy level diagrams can be estimated directly from the absorption spectra. This absence of CI between the near-UV and visible transitions of like symmetry follows from the large splitting (9600 cm^{-1}) of the HOMO levels. The gap between the LUMOs is smaller (1250 cm^{-1}); however, the orthogonality of each of the components of the visible and the near-UV manifolds also precludes strong CI effects.

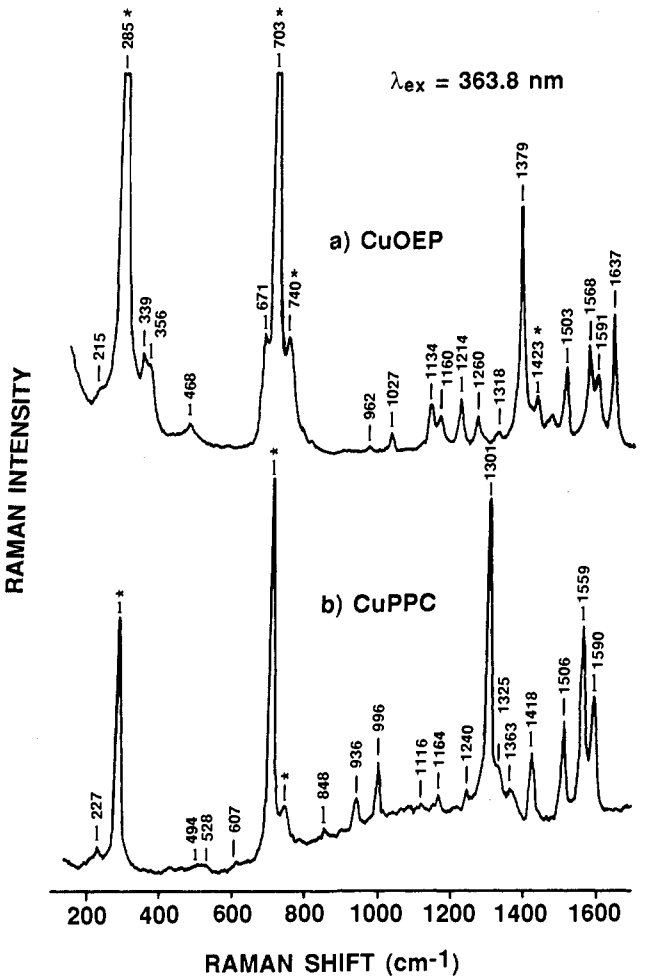

Figure 5. Resonance Raman spectra of CuOEP and CuPPC in CH_2Cl_2 at concentrations of approximately 0.1 and 0.2 mM, respectively. Laser powers at 363.8 nm were 20 and 10 mW, respectively. Solvent vibrations in this and Figures 6, 7, and 9 are marked with an asterisk.

Woodruff et al.[6] have suggested similar arguments to interpret UV–visible, MCD, and RR spectra of heme *a*. These authors argue that the trans disposition of a formyl and vinyl group in this porphyrin lift the x,y degeneracy of the porphyrin resulting in effective D_{2h} symmetry for this molecule. Earlier, Platt[20] and co-workers pointed out examples termed "long-field" molecules, in which configuration interaction was minimized. These include pyrene, biphenyl, and tetrahydroporphine. Although Platt[20a] speculated that there is most likely no pure long-field molecule, metalloporphycene may represent the best example of such thus far encountered.

Resonance Raman Spectra. Figure 5 displays Raman spectra obtained in resonance at 363.8 nm of CuOEP and CuPPC. Like the optical absorption spectra, these are superficially similar and both are dominated by intense features in the 1300–1650-cm^{-1} region. In the metalloporphyrin complex, CuOEP, these normal modes involve C=C and C=N stretching coordinates. Their large intensity is attributed to correspondingly large displacements along these normal coordinates in the $\pi \rightarrow \pi^*$ excited states of the porphyrin macrocycle. The frequencies of these vibrations are structure sensitive, i.e. they are dependent on the size and redox state of the central metal. The normal coordinate analyses[24] of NiOEP and CuOEP indicate that the dominant Raman-active

(22) (a) Obtained from the correlation tables in: Wilson, E. B.; Decius, J. C.; Cross, P. C. In *Molecular Vibrations: The Theory of Infrared and Raman Vibrational Spectra*; Dover Publications, 1955; Appendix X. Note that the C_2'' axes of MOEP are retained in MPPC (see Figure 1). (b) The effects of ring bromination and metal substitution on the individual MO energies will be more readily understood when calculations yielding orbital coefficients become available.

(23) (a) Caughey, W. S.; Deal, R. M.; Weiss, C.; Gouterman, M. *J. Mol. Spectrosc.* **1965**, *16*, 451–463. (b) Caughey, W. S.; Fujimoto, W. Y.; Johnson, B. P. *Biochemistry* **1966**, *5*, 3830–3843.

(24) (a) Abe, M.; Kitagawa, T.; Kyogoku, Y. *J. Chem. Phys.* **1978**, *69*, 4526–4534. (b) Gladkov, L. L.; Solovyov, K. N. *Spectrochim. Acta* **1986**, *42A*, 1–10. (c) Li, X.-Y.; Czernuszewicz, R. S.; Kincaid, J. A.; Stein, P.; Spiro, T. G. *J. Phys. Chem.* **1990**, *94*, 47–61. (d) Atamian, M.; Donohoe, R. J.; Lindsey, J. R.; Bocian, D. F. *J. Phys. Chem.* **1989**, *93*, 2236–2243. (e) Li, X. Y.; Czernuszewicz, R. S.; Kincaid, J. A.; Su, O. Y.; Spiro, T. G. *J. Phys. Chem.* **1990**, *94*, 31–47.

Table II. Resonance Raman Depolarization Ratios, $\rho = I_\perp/I_\parallel$, for CuPPC[a]

Raman shift (cm^{-1})	excitation wavelengths, λ_{ex} (nm)			
	406.7	568.2	613.0	630.0
1590	0.3	0.2	0.2	0.3
1559	0.4	0.5	0.5	0.4
1506	0.4	0.3	0.3	0.3
1417	0.5*	0.4	0.5	0.5
1363 (w)	0.1	(w)	0.4	(w)
1326	(w)	(w)	0.4	(w)
1301	0.5	0.4	0.5	0.4
1240	0.2	(w)	0.2	0.3
1165	0.6*	(w)	(w)	(w)
1116	0.3	0.3	0.4	0.4
1060	0.5	(w)	(w)	(w)
996	0.2	0.3	0.3	0.3
936	(w)	0.6	1.0 (w, ?)	1.0 (w, ?)

[a] An asterisk indicates that the ρ value may be anomalously high due to contribution from an underlying depolarized solvent band. w = weak intensity making measurement of ρ unreliable.

high-frequency normal modes of CuOEP (Figure 2, insert) include two primarily νC_aC_m stretches, ν_{10} (1637 cm^{-1}, b_{1g}) and ν_3 (1503 cm^{-1}, a_{1g}), and two primary νC_bC_b stretching motions, ν_2 (1591 cm^{-1}, a_{1g}) and ν_{11} (1568 cm^{-1}, b_{1g}). The ν_4 (1379 cm^{-1}, a_{1g}) mode of metalloporphyrins is predominantly a νC_aN, δC_aC_m "breathing" motion of the macrocycle.

In order to determine the symmetry of the principal vibrations of the CuPPC spectrum in Figure 5b we present (below) depolarization ratios from polarized RR spectra of CuPPC excited at 406.7, 568.2, 613.0, and 630.0 nm. RR spectra of specifically deuterated forms of NiPPC are also shown below and are used to suggest tentative vibrational assignments of the normal modes. Comparison of the NiPPC to the CuPPC spectra allows us to identify structure vibrations.

Symmetry and the Resonance Raman Depolarization Ratio. The skeletal structure of the metalloporphycene belongs to the D_{2h} point group (Figure 1). The x and y symmetry axes are oriented through the bridging positions, but not through the pyrrole groups, as in the metalloporphyrin (D_{4h}). For the 37-member structure in which all substituents are considered point masses, 51 Raman-active and 45 IR-active fundamental vibrations should occur. In the resonance Raman spectrum we expect to observe only in-plane vibrations, as these will be strongly enhanced by the in-plane $\pi \rightarrow \pi^*$ electronic transitions of the macrocycle. There should be 35 in-plane Raman-active fundamentals: 18 a_g and 17 b_{1g}. These can be readily distinguished by measurement of the Raman depolarization ratio, ρ. For totally symmetric a_g vibrations, $0 < \rho < {}^3/_4$ and the value should approach ${}^1/_3$ on resonance. For b_{1g} modes, $\rho \geq {}^3/_4$; that is, the latter modes can assume anomalous polarization if the scattering tensor is a mixture of symmetric and antisymmetric contributions.[25] Figure 6 shows polarized RR scattering from CuPPC obtained by using laser excitation at 406.7 and 613.0 nm. Similar spectra (not shown) were measured with λ_{ex} = 568.2 and 630.0 nm, and depolarization ratios for the most intense bands are collected in Table II. The table shows that, although some differences in the relative intensities occur, all of the major RR bands observed are present at each employed λ_{ex} and display ρ in the 0.2–0.5 range. Further, within the error limits of our measurements (±0.1), the ρ values for the individual vibrations do not in general display appreciable dispersion. Thus, for the metalloporphycene we observe only polarized modes and we do not observe the distinctive inverse or anomalous polarization phenomenon present in the RR scattering of the metalloporphyrin.[26] By their depolarization ratios, we assign all of these vibrations to the totally symmetric representation, a_g.

Vibronic Coupling. Although the one-electron $\pi \rightarrow \pi^*$ states of the metalloporphycene do not show strong electronic coupling,

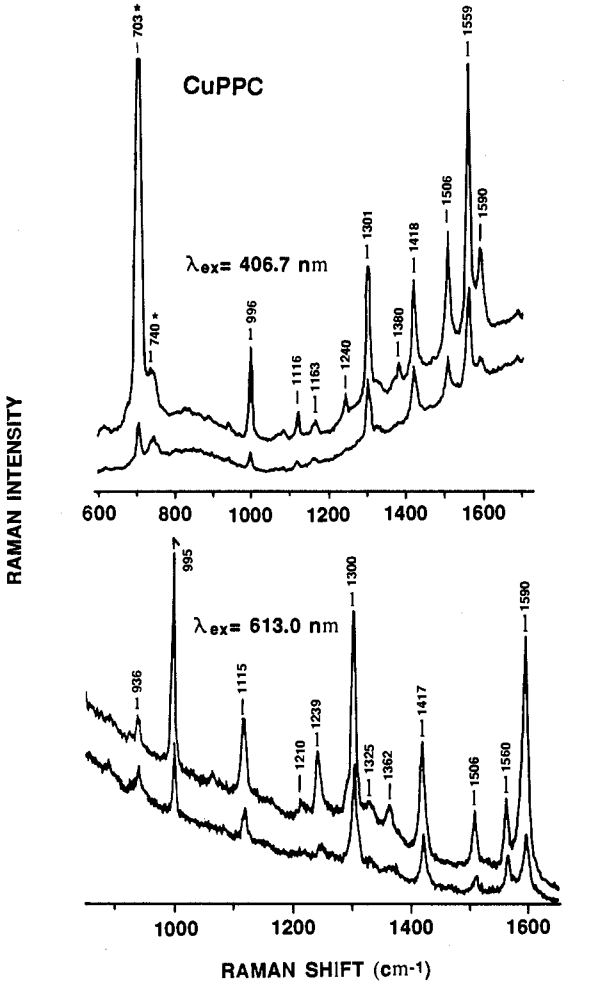

Figure 6. Polarized resonance Raman spectra of CuPPC in CH_2Cl_2 at 406.7 and 613.0 nm. Concentrations were approximately 0.5 and 0.3 mM and laser powers 40 and 100 mW, respectively. In each spectrum, the top trace represents $I_\parallel$ and the bottom trace represents $I_\perp$.

i.e., weak CI, vibronic coupling is still conceivable. Under D_{2h} symmetry $B_{2u} \times B_{3u} = b_{1g}$. Thus the b_{1g} modes can couple these electronic transitions via a Herzberg–Teller (HT) mechanism. Electronic transitions of like symmetry can couple via a_g modes; thus, it is possible for totally symmetric modes to exhibit HT activity. Indeed, vibronic activity of a_{1g} modes has been reported for metalloporphyrins.[27] The relative oscillator strengths of the visible and near-UV bands apparent from the absorption spectrum in Figure 2, however, imply an absence of HT coupling in MPPC compounds. That is, in metalloporphyrins, HT coupling of a formally forbidden transition (the Q band) to an allowed one (the Soret band) results in a smaller ratio of visible to near-UV oscillator strengths.[17] At any rate, because we do not observe any anomalously polarized modes in the RR spectra we find no conclusive evidence of HT coupling and we speculate that the scattering derives primarily from an Albrecht *A*-term (Franck–Condon) mechanism. Since no degenerate representations are contained in the D_{2h} point group, Jahn–Teller (JT) coupling is not expected. In view of the above we assign all of the 18 vibrations listed for CuPPC in Table III to the totally symmetric representation, a_g. Owing to the apparent sparseness of vibronic coupling, the spectra of NiPPC and CuPPC are remarkably simple. This is in contrast to the case for metalloporphyrins, where

(25) (a) Clark, R. J. H.; Stewart, B. *Struct. Bonding* **1979**, *36*, 1–80. (b) Bernstein, H. J. *Phil. Trans. R. Soc. London A* **1979**, *293*, 287–302.
(26) Spiro, T. G.; Strekas, T. C. *Proc. Natl. Acad. Sci. U.S.A.* **1972**, *69*, 2622–2626.
(27) (a) Shelnutt, J. A.; O'Shea, D. C.; Yu, N.-T.; Cheung, L. D.; Felton, R. H. *J. Chem. Phys.* **1976**, *64*, 1156–1165. (b) Shelnutt, J. A.; Cheung, L. D.; Chang, R. C. C.; Yu, N.-T.; Felton, R. H. *J. Chem. Phys.* **1977**, *66*, 3387–3398. (c) Nishimura, Y.; Hirakawa, A. Y.; Tsuboi, M. *J. Mol. Spectrosc.* **1977**, *68*, 335–358. (d) Shelnutt, J. A. *J. Chem. Phys.* **1981**, *74*, 6644–6657.

Table III. Raman Vibrational Frequencies (cm^{-1}) of $M^{II}PPC$ Complexes

CuPPC	CoPPC[a]	NiPPC	NiPPC-d_4-(py)	NiPPC-d_4-(et)	assignment
1590	1612	1625	1620	1625	νCC(py)
1559	1571	1579	1574	1565	νCC(et,py)
1506	1515	1520	1509	1518	νCC(py)
1417	1407	1410	1403	1357	νC_eC_e, δC_eH
1363	1368	1368	1368 (w)	1368 (w)	νC_aN
1326		1327	1327	1327	νC_aN
1301	1299	1305	1302	1305	$\nu C_{a'}N$
			1270[b]		
1240		1231	1227	1187	δC_eH (small %)
1165	1164	1167	925	1167	$\delta C_{b'}H$ (large %)
1116		1120	1122	1118	
1065 (w)		1064 (w)			
			1085[b]		
			1016[b]		
996	995	996		996	δC_α-propyl
936	944	944		931	
848		846	~850 (w)	813 (w)	
607	607	608	602	606	
528					
494 (w)					
227					

[a] The CoPPC spectra (not shown) indicated some residual free base present in the sample. These contributions may skew the frequencies presented here despite efforts to subtract them from the data. [b] These frequencies most likely represent normal modes of significantly different character than those of the natural abundance sample.

the CI-induced excited states are extensively affected by both JT and HT couplings resulting in RR spectra that are exceedingly rich in vibronic information.[25-27]

Effects of Selective Deuteration and Metal Substitution on Raman Frequencies. Figure 7 shows the RR spectra of NiPPC, NiPPC-d_4(py), and NiPPC-d_4(et). The latter two complexes have deuterium substituted for hydrogen at the $C_{b'}$ pyrrole positions and at the C_e ethylene positions, respectively. The frequencies of the Raman bands are collected in Table III along with those measured for CuPPC (Figures 5b and 6) and CoPPC (data not shown). Tentative partial assignments based on the isotope shifts are included. In general, more complete vibrational analysis will require additional isotopic substitutions accompanied by a normal coordinate calculation, and the data presented here will be useful in such an endeavor.

In the region above 1400 cm^{-1} the intense RR bands are clearly isotope sensitive and easily correlated. The 5–11-cm^{-1} shifts upon d_4(py) but not d_4(et) substitution clearly indicate that the 1625- and 1520-cm^{-1} vibrations of NiPPC involve the $C_{b'}$ atom and not the ethylene bridge carbons (C_e). Thus, they are most likely localized on the pyrrole rings and/or across the $C_{a'}C_{a'}$ bond. On the other hand, the features at 1579 and 1410 cm^{-1} shift in both isotopically substituted species, suggesting delocalized motions involving both pyrrole and ethylene bridge carbons. The mode at 1410 cm^{-1} shifts more dramatically upon d_4(et) substitution and is hence assigned a large percentage of νC_eC_e and possibly some δC_eH character. The bands in the 1300–1400-cm^{-1} region shift little upon deuteration at the outer ring carbons and are assigned to C=N stretches.

Below 1300 cm^{-1} the Raman features are less intense and the normal modes likely undergo changes in composition upon deuteration. Thus, it is difficult to correlate features and ascertain the internal coordinates involved based purely on isotopic shifts. In the d_4(py) derivative, features appear at 1270, 1085, 1016, and 925 cm^{-1} that are not easily associated with vibrations of the natural abundance sample. This is also true for the 1187-cm^{-1} feature in the d_4(et) sample. Some suggestions are presented in Table III, but these must be considered tentative. For example, the 925-cm^{-1} feature in the NiPPC-d_4(py) spectrum is most likely due to a δC_bD motion. In NiOEP, NiTPP, and CuTPP (TPP = tetraphenylporphyrin) the δC_mH and δC_bH motions, respectively, can cause shifts upon deuteration ranging from −30 to −400 cm^{-1}, depending on the potential energy distribution (P.E.D.) of the normal mode.[24] Hence, correlating the 925-cm^{-1} feature with the 1167-cm^{-1} band present in both NiPPC and NiPPC-d_4(et) is

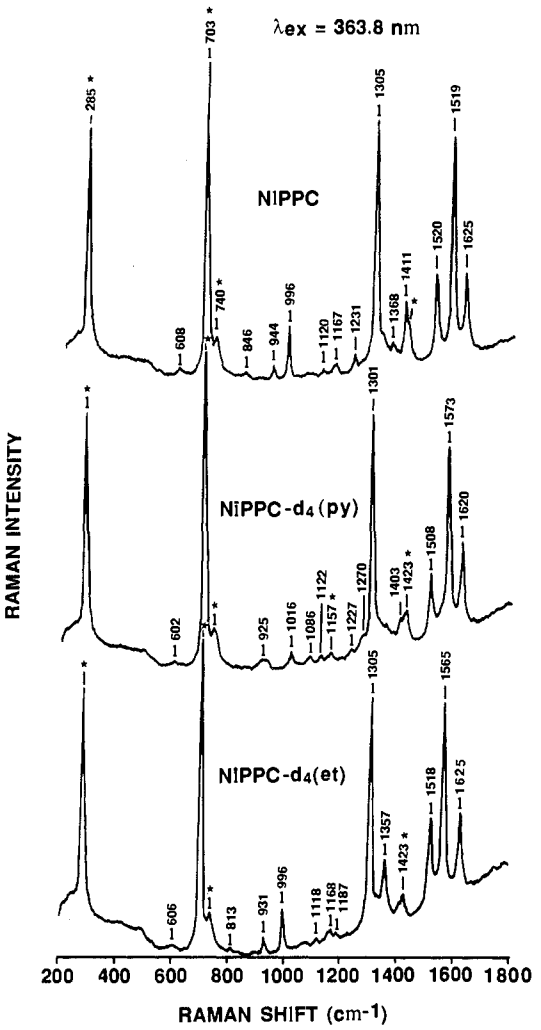

Figure 7. RR spectra of 0.2 mM CH_2Cl_2 solutions of NiPPC derivatives. Laser power at 363.8 nm was 30 mW.

reasonable. The 1410-cm^{-1} vibration of NiPPC can be compared to a mode at 1504 cm^{-1} of both CuTPP and NiTPP that has been assigned by Atamian et al.[24d] and Li et al.[24e] to a mixture of νC_bC_b and δC_bH motions. The deuterium shifts of −44 and −47 cm^{-1} reported for these porphyrin vibrations[24d,e] are similar to the −53-cm^{-1} shift we observed for NiPPC upon deuteration at the ethylene bridge carbons. CuTTP and NiTPP also have a mode around 1375 cm^{-1} displaying approximately a −40 cm^{-1} deuterium shift. This mode is likely a mixture of the νC_aC_b and C_aN or δC_bH coordinates.[24d,e] By analogy to these assignments, based on the frequency and isotopic shift, we assign the 1410-cm^{-1} feature of NiPPC to a mixture of νC_eC_e, δC_eH, and, owing to the smaller −7-cm^{-1} shift on d_4(py) substitution, possibly some $\nu C_{a'}C_{b'}$ or $\nu C_{a'}N$ motion. Finally, the 996-cm^{-1} mode probably involves the propyl substituents similar to the 1025-cm^{-1} vibration in NiOEP.[24a,c] Incorporation of deuterium at the $C_{b'}$ position most likely causes a change in normal mode composition resulting in a new vibration at 1016 cm^{-1} (and possibly also at 1085 cm^{-1}). This could well result from coupling of the $\delta C_{b'}D$ vibration, which has shifted into the 900–1000-cm^{-1} region, with the 996-cm^{-1} mode. The $\delta C_{b'}D$ could then derive some intensity from the 996-cm^{-1} vibration resulting in the features at 925 and 1016 cm^{-1} observed in the spectrum of NiPPC-d_4(py). Similar coupling may also occur for the 944-cm^{-1} vibration, as it cannot be found in the NiPPC-d_4(py) spectrum. This vibration undergoes an isotopic shift upon d_4(et) substitution, whereas the 996-cm^{-1} vibration does not, indicating that they are localized in different areas of the macrocycle.

Structure-Sensitive Vibrations. In metalloporphyrins the vibrations in the 1400–1700-cm^{-1} range are distinctly dependent on the central metal. This is due to variations in the size of the

porphyrin core in response to metal substitution. Spaulding et al.[28] identified the relevant structural parameter to be the center to pyrrole nitrogen distance, d_{CtN}. Huong and Pommier[29] quantified the relationship between vibrational frequency and d_{CtN}, and subsequent work extended the correlations to a large number of vibrations of a variety of metalloporphyrin[10a,30] complexes. Because the relationship between frequency and core size is dependent on the P.E.D. of the vibration, such analysis has been used to support vibrational assignments in metallochlorins[4a,d] and in the π-cation radicals of metalloporphyrins[10a] and metallochlorins.[10b] Comparison of the crystal structures of Ni^{II} and Mg^{II} porphyrins[31] shows that the C_aC_m and C_bC_b bond lengths change by 0.044 and 0.014 Å upon expansion of the porphyrin d_{CtN} from 1.958 to 2.055 Å. The lengthening of these bonds decreases the νC_aC_m and νC_bC_b frequencies. Thus, those normal coordinates involving νC_aC_m motion, followed by those involving νC_bC_b motion, show the steepest inverse slopes in the relationship between frequency and core size $\nu = K(A - d_{CtN})$.[29]

Table III lists frequencies for the Raman-allowed vibrations of Cu^{II}, Co^{II}, and Ni^{II} complexes of PPC. These demonstrate a metal dependence similar to that of the analogous OEP complexes. The vibrations at 1625, 1579, and 1520 cm^{-1} in NiPPC decrease by 35, 20, and 14 cm^{-1}, respectively, in CuPPC. This suggests that these vibrational frequencies are structure sensitive. The structural parameter that determines the vibrational frequencies cannot be identified with certainty until more crystal structures are determined. Correlation of vibrational frequency to metalloporphycene structure will be complicated by the apparent dependence of the core skeletal structure of the porphycene ligand upon the nature and position of the peripheral substituents.[2e] This is in contrast to the case for metalloporphyrins,[34] where the relative invariance of the core size of different porphyrins complexed to the same metal has been exploited extensively in establishing correlations of vibrational frequencies to d_{CtN}.[28]

Given the above cautions, a preliminary analysis of the available structural and vibrational data suggests that the three highest RR frequencies of the PPC macrocycle are, nevertheless, approximately linearly dependent on the center-to-nitrogen distance. Table IV collects the structural data for PPC compounds and compares it to that of analogous porphyrins. Measurements (not shown) of H_2PPC, H_2PPC-d_4(py), and H_2PPC-d_4(et) reveal that the three highest RR frequencies of the free base PPC at 1606, 1559, and 1505 cm^{-1} derive from normal modes with qualitatively similar P.E.D.'s to those of the metallo-PPC complexes. Thus, we can use these points to estimate K and A parameters for a structural correlation of porphycene vibrational frequency to core size for each of these modes (Table IV).

Comparison of these estimated structural parameters to those of porphyrins (see Table IV and ref 28–34 and references therein) suggests interesting generalizations. The porphycene macrocycle is in general smaller, more rigid, and less able to expand than the porphyrin ring. This is reflected by the fairly high K values (inverse slope) estimated for PPC vibrations compared to those of typical high-frequency porphyrin modes.[10a,29,30] Also, the core

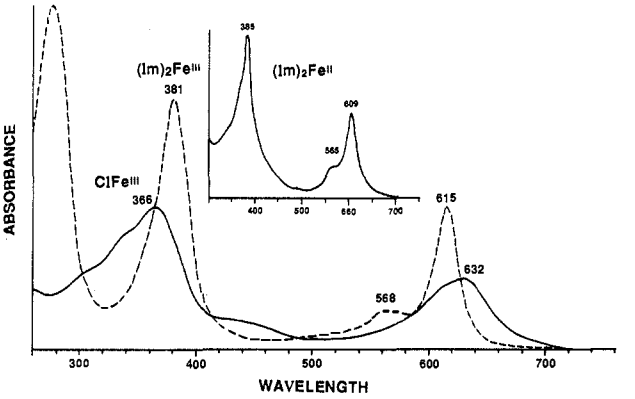

Figure 8. UV–visible absorption spectra of FePPC derivatives in CH_2Cl_2. Conditions were as described in Figure 2, and the ferrous sample (inset spectrum) was prepared with hydrazine hydrate as a reductant as described in Materials and Methods. The absorption at 280 nm in the spectrum of the $(Im)_2Fe^{III}$ sample is from excess *N*-methylimidazole.

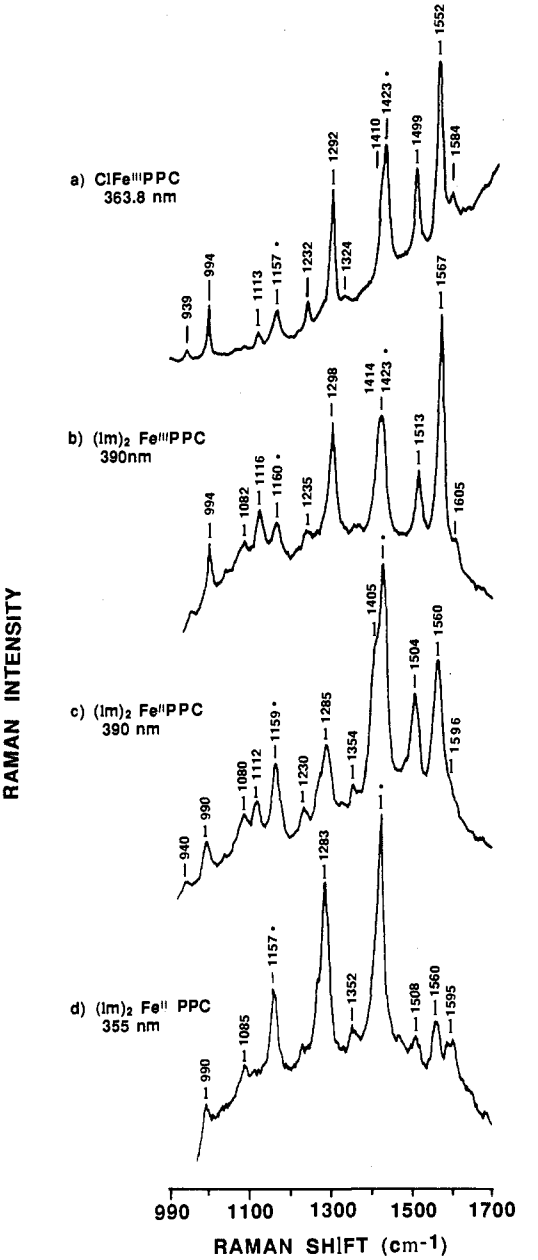

Figure 9. RR spectra of Fe^{III} and Fe^{II} complexes of PPC. Concentrations in CH_2Cl_2 were approximately 0.1 mM and laser powers were typically 20 mW. Spectrum a was measured with a different diode array detector than spectra b–d.

(28) Spaulding, L. D.; Chang, C. C.; Yu, N.-T.; Felton, R. H. *J. Am. Chem. Soc.* **1975**, *97*, 2517–2525.
(29) Huong, P. V.; Pommier, J.-C. *C. R. Acad. Sci. Ser. C* **1977**, *285*, 519–522.
(30) (a) Callahan, P. M.; Babcock, G. T. *Biochemistry* **1981**, *20*, 952–958. (b) Parthasarathi, N.; Hasen, C.; Yamaguchi, S.; Spiro, T. G. *J. Am. Chem. Soc.* **1987**, *109*, 3865–3871.
(31) (a) Cullen, D. L.; Meyer, E. F. *J. Am. Chem. Soc.* **1974**, *96*, 2095–2102. (b) Timkovich, R.; Tulinsky, A. *J. Am. Chem. Soc.* **1969**, *91*, 4430–4432.
(32) From unpublished EXAFS measurements by L. R. Furenlid, M. R. Renner, and J. Fajer. A related study of NiPPC showed excellent agreement between the EXAFS and X-ray data: see: Furenlid, L. R.; Renner, M. R.; Smith, K. M.; Fajer, J. *J. Am. Chem. Soc.* **1990**, *112*, 1634–1635.
(33) Silvers, S.; Tulinsky, A. *J. Am. Chem. Soc.* **1964**, *86*, 927–928.
(34) Scheidt, W. R.; Lee, Y. T. *Struct. Bonding* **1987**, *64*, 1–70 and references therein.
(35) (a) Smith, D. W.; Williams, R. J. P. *Struct. Bonding* **1969**, *7*, 1–45. (b) Adar, F. In *The Porphyrins*; Dolphin, D., Ed.; Academic: New York, 1979; Vol. III, pp 167–209.
(36) Neya, S.; Chang, C. K.; Vogel, E. et al., manuscript in preparation.

Table IV.

(A) Core Sizes of PPC and Analogous Porphyrin Complexes

	d_{CtN} (Å)			
	PPC	ref	porphyrin	ref
Ni	1.896	2a	1.958	28, 31a
Cu	1.94 ± 0.01	32	2.000	28
H_2	1.927	2a	2.065	33

(B) Estimates of Structural Parameters for MPPC Vibrational Frequencies

NiPPC vibration (cm^{-1})	K (cm^{-1}/Å)	A (Å)
1625	760	4.03
1579	490	5.12
1520	350	6.26

size of the free base porphycene falls within the range of these metal complexes, whereas the free base porphyrin has a larger core size than the metalloporphyrin complexes considered here. This relatively contracted core size for H_2PPC is the result of exceptionally strong internal hydrogen bonds between the imine pyrrole nitrogen atoms and the free base protons.[1,2e]

Iron Complexes. Figure 8 illustrates the UV–visible spectral changes manifested during conversion of the five-coordinate ferric chloride complex to a 6-coordinate ferric bis(*N*-methylimidazole), $(Im)_2$, complex. The spectrum of $(Im)_2Fe^{III}$PPCCl (Figure 8) is quite similar to that of CuPPC (Figure 2); however, the structure in the near-UV band is less well resolved. The $ClFe^{III}$PPC spectrum is more complex than that of $(Im)_2Fe^{III}$PPCCl, suggesting that the $\pi \rightarrow \pi^*$ excited states of the ring (B_{2u} and B_{3u} in D_{2h} symmetry) interact with $\pi \rightarrow d_{yz}, d_{xz}$ charge-transfer excited states (also B_{2u} and B_{3u}). These CT states are likely produced from b_{1u} (porphycene) $\rightarrow$ b_{3g},b_{2g} (iron) transitions analogous to the a_{2u} (porphyrin) $\rightarrow$ e_g (iron) transitions of D_{4h} hemes.[35] As the latter do not occur in low-spin Fe^{III} systems, their presence in the absorption spectrum[21] of $ClFe^{III}$PPC is consistent with a spin state higher than $S = {}^1/_2$. Analogous ferric porphyrin complexes exhibit spectral trends qualitatively similar to those in Figure 8.

By analogy to $ClFe^{III}$ porphyrins, we at first expected a pure $S = {}^5/_2$ high-spin state for $ClFe^{III}$PPC; however, magnetic susceptibility measurements indicated that substantial $S = {}^3/_2$ intermediate-spin character exists.[36] The smaller core size of porphycene presumably increases the splitting of the $d_{x^2-y^2}$ level from the other iron orbitals making the $S = {}^5/_2$ state less accessible than in porphyrin complexes; this causes a quantum-mechanically mixed $S = {}^5/_2$ and ${}^3/_2$ spin state for the porphycene complex.

In iron porphyrins the vibrational frequencies of the macrocycle are known to be sensitive to the ligation, spin, and oxidation state of the Fe. This situation has been extensively exploited by RR study of heme proteins.[12] It is of interest to determine if a similar situation exists for iron porphycenes. Figure 9 compares RR spectra of the five-coordinate $ClFe^{III}$PPC and six-coordinate $(Im)_2Fe^{III}$PPC and $(Im)_2Fe^{II}$PPC. The EPR spectrum of the six-coordinate ferric complex confirms an $S = {}^1/_2$ spin state for the iron atom. The Raman bands of $(Im)_2Fe^{III}$PPCCl at 1298, 1513, 1567, and 1605 cm^{-1} are clearly higher in frequency from the analogous features in the ferric chloride complex. This indicates that the conformation of the porphycene macrocycle is more contracted in the $(Im)_2Fe^{III}$ complex than in the $ClFe^{III}$ adduct.

Reduction of the $(Im)_2Fe^{III}$ complex to $(Im)_2Fe^{II}$ with hydrazine hydrate affords the UV–visible spectrum inset in Figure 8. The RR spectrum excited at 390 nm of the reduced product appears in Figure 9c, while the spectrum at λ_{ex} = 355 nm of the same compound in the presence of excess reductant appears in Figure 9d. The spectra are consistent with metal-centered reduction. The 14-cm^{-1} decrease from 1298 to 1284 cm^{-1} upon reduction is larger than the 7–9-cm^{-1} decrease exhibited by the vibrations in the 1400–1700-cm^{-1} range. While the latter reflect the macrocycle expansion attributable to the larger ionic radius of Fe^{II} than Fe^{III}, the decrease in frequency of the mode around 1300 cm^{-1} is much larger than expected by comparison to the Ni^{II} and Cu^{II} complexes. Consequently, this feature appears analogous to the ν_4C_aN mode of hemes, the "oxidation state marker". The porphycene mode is likely a νC_aN or $\nu C_{a'}N$ motion, and these data suggest overlap between the porphycene $b_{3g}(\pi^*)$ and $b_{2g}(\pi^*)$ orbitals and the iron $b_{3g}(d_{yz})$ and $b_{2g}(d_{xz})$ orbitals, analogous to the situation in iron porphyrins.[12,37] Reduction of the metal to Fe^{II} most likely leads to population of the macrocycle π^* orbitals and weakening of the C_aN and/or $C_{a'}N$ bonds.

Acknowledgment. We thank Drs. A. Salehi, M. Atamian, S. Neya, P. O. Sandusky, and R. J. Donohoe for technical assistance and discussion. W.A.O. thanks Professor G. T. Babcock for valuable discussion and generous support from NIH Grant GM25480 and Dr. P. M. Hunt for REF funds. C.K.C. acknowledges support from NIH Grant GM36520 and Dr. J. Fajer for unpublished results of EXAFS of CuPPC. The NMR data were obtained on instrumentation purchased in part with funds from NIH Grant RR04750 and from NSF Grant CHE-88-00770.

(37) Kitagawa, T.; Abe, M.; Kyogoku, Y.; Ogoshi, H.; Sugimoto, H.; Yoshida, Z. *Chem. Phys. Lett.* **1977**, *48*, 55–58.